Research Square

Preprints are preliminary reports that have not undergone peer review.
They should not be considered conclusive, used to inform clinical practice,
or referenced by the media as validated information.

Interplanetary scintillation observations and MHD simulation of successive coronal mass ejections in early May 2024

Kazumasa Iwai

k.iwai@isee.nagoya-u.ac.jp

Nagoya University https://orcid.org/0000-0002-2464-5212

Daikou Shiota

National Institute of Information and Communications Technology Applied Electromagnetic Research Institute: Kokuritsu Kenkyu Kaihatsu Hojin Joho Tsushin Kenkyu Kiko Sogo Test Bed Kenkyu Kaihatsu Suishin Center

Ken'ichi Fujiki

Nagoya University: Nagoya Daigaku

Hirofumi Isogai

Nagoya University: Nagoya Daigaku

Research Article

Keywords: interplanetary scintillation, coronal mass ejection, space weather forecasting, magnetohydrodynamics

Posted Date: September 29th, 2026

DOI: https://doi.org/10.21203/rs.3.rs-11033519/v1

License: This work is licensed under a Creative Commons Attribution 4.0 International License.
Read Full License

Abstract

In early May 2024, multiple coronal mass ejections (CMEs) were launched in close succession during a period of exceptionally high solar activity and were followed by an extreme geomagnetic storm. We investigated the large-scale inner-heliospheric structure associated with this event using 327 MHz interplanetary scintillation (IPS) observations obtained with the radio telescope system operated by the Institute for Space–Earth Environmental Research, Nagoya University, together with the SUSANOO-CME global magnetohydrodynamic simulation. On 9–10 May 2024, particularly on 10 May, enhanced IPS signals were detected from numerous radio sources over a broad range of solar elongations before the main geomagnetic disturbance at Earth. Relative to quiet-day conditions, both the number of sources showing enhanced scintillation and the spatial extent of the enhancement increased markedly, indicating the presence of a spatially extended density disturbance in the inner heliosphere. The synthetic IPS distribution broadly reproduced the observed spatial pattern as signatures of adjacent or partially merged compression regions formed during the propagation and possible interaction of successive CMEs. Although residual RFIs and discrepancies in the modeled timing and geometry limit detailed correspondence along individual lines of sight, the observations and simulation are consistent at the large scale. This case study shows that IPS observations can detect compound and spatially extended CME-related disturbances before their arrival at Earth, illustrating the value of IPS for monitoring complex heliospheric structures associated with events that subsequently produce severe space weather.

1. Introduction

Coronal mass ejections (CMEs) are one of the primary drivers of severe space weather in the Sun–Earth system. Fast CMEs propagating through interplanetary space compress the ambient solar wind and can generate shocks, sheath regions, and complex ejecta, sometimes leading to intense geomagnetic disturbances when they reach Earth (e.g., Webb and Howard, 2012). In particular, successive eruptions from the same active region can interact during propagation, producing enhanced plasma compression and more complicated heliospheric structures than those associated with isolated CMEs (Liu et al., 2014; Lugaz et al., 2017). Detecting such evolving structures in the inner heliosphere is therefore important for understanding extreme space weather events and for improving situational awareness before their arrival at Earth.

Interplanetary scintillation (IPS) is a radio-scattering phenomenon caused by density irregularities in the solar wind and provides a remote-sensing technique for monitoring heliospheric plasma structures over a wide range of elongations (Hewish et al., 1964; Gapper et al., 1982). Because CME fronts and compressed regions contain enhanced density fluctuations, they can produce detectable IPS signatures during propagation between the Sun and Earth (e.g., Manoharan, 2006). Previous studies have shown that IPS observations are sensitive to CME-related disturbances in the inner heliosphere and can complement white-light coronagraph observations near the Sun and in situ measurements near Earth (Manoharan, 2006; Glyantsev et al., 2015; Iwai et al., 2019). In this sense, IPS offers a unique

observational capability for tracking CME-associated density structures in the inner heliosphere, where direct observations are limited.

IPS data have been used to reconstruct the global heliospheric structure by means of tomography techniques (Jackson et al., 1998; Kojima et al., 1998). More recently, the interpretation of IPS observations has been enhanced through comparison with global magnetohydrodynamic (MHD) simulations (Iwai et al., 2019 and references therein). For example, IPS data have been used for MHD-based tomography (Hayashi et al., 2003) and as additional constraints on the inner boundary conditions of global MHD simulations (Jackson et al., 2015; Yu et al., 2015). In Iwai et al. (2019), a forward-fitting technique was developed to interpret IPS data through comparison with MHD simulations. Numerical models provide the three-dimensional heliospheric context of CME propagation and make it possible to calculate synthetic IPS responses along the corresponding lines of sight. Such comparisons have been used to investigate the geometry and evolution of CME-related structures and to assess whether observed IPS enhancements can be explained by dense regions formed during interplanetary propagation. In particular, the combination of the SUSANOO-CME simulation framework (Shiota et al., 2014; Shiota and Kataoka, 2016) and IPS observations has proven useful for examining how CME-driven structures develop in the heliosphere (Iwai et al., 2019, 2021, 2023). SUSANOO-CME has also been used operationally at NICT for space weather forecasting, including during the May 2024 event (Sakaguchi et al., 2026).

In early May 2024, multiple major eruptions occurred during a period of exceptionally active solar conditions. Several CMEs were launched in close succession and were followed by an intense geomagnetic storm on 10–11 May 2024, accompanied by widespread auroral activity (e.g., Hayakawa et al., 2025; Spogli et al., 2024; Mlynczak et al., 2024; Tulasi Ram et al., 2024; Sakaguchi et al., 2026). The event attracted broad attention because the geospace impact was unusually strong and because the eruptions were likely not independent, but interacted with one another during propagation (Liu et al., 2024; Razquin et al., 2025). Strong IPS responses were detected on 9–10 May, before the main geomagnetic disturbance, and these responses were distributed over many lines of sight, suggesting the presence of large-scale compressed plasma structures in interplanetary space.

In this paper, we report 327 MHz IPS observations of the May 2024 CME event obtained with the radio telescope operated by the Institute for Space - Earth Environmental Research (ISEE), Nagoya University, and compare them with results from the SUSANOO-CME MHD simulation. We focus on the spatial distribution of enhanced IPS signals observed on 10 May 2024 and examine whether these features can be interpreted as signatures of dense regions formed by successive CME propagation and interaction. Rather than aiming at a comprehensive reconstruction of the entire event, this study presents an observational case report demonstrating that IPS measurements can detect complex CME-related structures relevant to severe space weather before their arrival at Earth.

2. Instruments, Data, and Simulation

2.1 IPS Observations

The interplanetary scintillation (IPS) observations analyzed in this study were carried out using the 327 MHz radio telescope system operated by the Institute for Space-Earth Environmental Research (ISEE), Nagoya University. The system consists of three observing sites in Japan, located at Toyokawa, Kiso, and Fuji, and has been used for routine IPS monitoring of the solar wind and interplanetary disturbances. In this study, we mainly used data obtained with the Toyokawa antenna of the IPS observation system (Tokumaru et al., 2011). The observing frequency is 327 MHz, which provides sensitivity to density fluctuations associated with solar wind transients, including coronal mass ejections (CMEs), in the inner heliosphere (Manoharan, 2006). For the present study, we focus on observations obtained during late April and early May 2024, with particular emphasis on 10 May 2024, when unusually strong IPS responses were detected prior to the major geomagnetic disturbance at Earth. During this period, approximately 70 radio sources were observed each day near the local meridian during daytime hours in Japan.

The raw intensity time series were processed using the standard IPS analysis procedure. Radio frequency interference (RFI) was mitigated by filtering of impulsive components, and the time series were then used to evaluate the scintillation level of each radio source. Following the conventional IPS analysis, we derived the relative scintillation enhancement (g-level), defined as the ratio of the observed scintillation level to the typical scintillation level for the same source at the corresponding solar elongation (Gapper et al., 1982). Values larger than unity can indicate enhanced scattering relative to the nominal solar wind condition.

2.2 MHD Simulation and Synthetic IPS Comparison

To interpret the IPS observations, we compared them with results from the SUSANOO-CME magnetohydrodynamic (MHD) simulation (Shiota and Kataoka, 2016). SUSANOO-CME is a global heliospheric MHD model that solves the time-dependent plasma evolution in three-dimensional space while continuously injecting the background solar wind from the inner boundary at 25 solar radii (Rs). In this framework, CMEs are represented as spheromak structures and introduced as additional eruptive structures at the inner boundary, enabling the propagation and interaction of multiple events to be examined within a global heliospheric context. The purpose of the simulation in this paper is not to reproduce every detail of the event perfectly, but to examine whether the large-scale distribution of enhanced IPS signals can be explained by dense structures formed during the propagation of successive CMEs. The simulation results therefore serve as a physical reference for interpreting the IPS pattern, especially in relation to plasma compression and possible CME–CME interaction in interplanetary space. In the present study, the simulation was configured to represent the sequence of CMEs associated with the May 2024 event, using CME parameters roughly estimated from solar and in situ observational constraints. A full list of the CME input parameters is provided in Table 1.

Table 1
Input parameters of the 15 CMEs used in the SUSANOO-CME simulation. Longitude and Latitude denote the heliocentric longitude and latitude of the CME source region, respectively. CMEVEL represents the initial speed of the CME, MAGFLUX the magnetic flux assigned to the injected CME structure, and RWIDTH and AWIDTH the radial and angular widths of the CME, respectively.

No.	Date (UT)	Time (UT)	Longitude (deg)	Latitude (deg)	CMEVEL (km s^{-1})	MAGFLUX (Mx)	RWIDTH (Rs)	AWIDTH (deg)
1	2024-05-08	05:09	12.0	-21.0	900.0	8.0e + 20	4.0	90.0
2	2024-05-08	12:04	12.0	-21.0	800.0	7.0e + 20	4.0	90.0
3	2024-05-08	21:40	18.0	-21.0	1050.0	1.6e + 21	4.0	90.0
4	2024-05-09	09:13	24.0	-20.0	1300.0	1.0e + 21	4.0	90.0
5	2024-05-09	17:44	29.0	-17.0	1350.0	5.0e + 20	4.0	90.0
6	2024-05-10	06:54	35.0	-18.0	1100.0	2.0e + 21	4.0	90.0
7	2024-05-10	20:03	-5.0	-20.0	800.0	5.0e + 20	4.0	90.0
8	2024-05-11	01:23	45.0	0.0	1800.0	2.0e + 21	6.0	90.0
9	2024-05-11	15:25	51.0	-18.0	1050.0	6.0e + 20	4.0	60.0
10	2024-05-13	09:44	81.0	-17.0	1800.0	2.1e + 21	6.0	90.0
11	2024-05-13	11:00	-40.0	-5.0	500.0	1.0e + 20	4.0	90.0
12	2024-05-14	02:09	90.0	-17.0	900.0	1.0e + 21	4.0	60.0
13	2024-05-14	10:24	-38.0	25.0	830.0	5.0e + 20	4.0	90.0
14	2024-05-14	16:51	90.0	-16.0	1600.0	1.3e + 21	4.0	90.0
15	2024-05-14	17:38	-60.0	20.0	1200.0	8.0e + 20	4.0	90.0

To compare the simulation with the observations, synthetic IPS distributions were calculated from the MHD output (Iwai et al., 2019). For each observing time, the model plasma parameters along lines of sight from Earth were used to estimate the scattering amplitude and to construct a sky-plane map

analogous to the observed IPS distribution. In this study, the synthetic IPS response was derived based on the formulation of Young (1971), assuming that the electron density perturbation is proportional to the plasma density obtained from the MHD simulation. To obtain a synthetic IPS *g*-level, we took the ratio of the IPS amplitude calculated from the simulation including CMEs to that calculated from the background solar wind simulation without CMEs. This quantity can be regarded as a proxy for the observed IPS *g*-level, enabling a qualitative comparison of the spatial patterns with the observations.

3. Results

3.1 Overview of the May 2024 Event

In early May 2024, multiple major flares and coronal mass ejections (CMEs) occurred in rapid succession from active regions AR13663 and AR13664 (Hayakawa et al., 2025; Liu et al., 2024; Razquin et al., 2025). These CMEs propagated toward Earth and caused the most intense geomagnetic storm in the past two decades on 10–11 May. Auroral emissions were observed at unusually low latitudes, including over Japan (Hayakawa et al., 2025; Spogli et al., 2024; Mlynczak et al., 2024).

Because several fast CMEs were launched within a short period, they likely approached one another and interacted or partially merged during their propagation through interplanetary space (Liu et al., 2024; Razquin et al., 2025). The event should therefore be regarded not as the propagation of a single CME, but as a compound heliospheric disturbance composed of multiple ejecta and their associated compression regions.

3.2 IPS Observations

Figure 1 shows the IPS observations obtained on 29 April 2024, during relatively quiet solar wind conditions, and on 9 and 10 May during the event. Enhanced IPS responses began to appear around 9 May and became most prominent on 10 May. In particular, the number of radio sources exhibiting strong scintillation enhancement increased substantially on 10 May compared with the quiet-day observations. By 20 May, after the passage of the series of CMEs, the IPS response had returned to a level comparable to that observed on 29 April. A preliminary report of these observations was presented by Hayakawa et al. (2025).

Strong IPS responses were detected not only along lines of sight close to the Sun, but also toward many radio sources at relatively large solar elongations. This broad spatial distribution differs from the scintillation pattern produced by the normal background solar wind and suggests the presence of a large and spatially extended disturbance in interplanetary space. These results indicate that dense structures associated with the successive CMEs had formed over a broad region of the inner heliosphere before the onset of the main geomagnetic disturbance at Earth.

Figure 1. IPS sky maps before, during, and after the May 2024 CME event.

All-source IPS sky maps observed on (a) 29 April, (b) 9 May, (c) 10 May, and (d) 20 May 2024. The center of each panel corresponds to the Sun, and the horizontal and vertical axes indicate the east–west and north–south positions of the P-points (the points of closest approach of the lines of sight to the Sun), expressed in AU. Plus signs indicate lines of sight toward the observed radio sources. Diamonds represent IPS g-levels: red for ($g > 2.0$), green for ($1.5 < g < 2.0$), and blue for ($1.2 < g < 1.5$).

Standard RFI mitigation procedures were applied to the observational data. Radio signals within an approximately 10 MHz bandwidth centered at 327 MHz, which lies within a protected radio astronomy band, were detected and sampled at 10 kHz. The ISEE IPS observations include many relatively weak radio sources for which the gradual intensity variation associated with the source transit cannot be clearly identified in the observed intensity time series. For such sources, the signal is typically buried in the background noise, and the time series therefore appears nearly noise-like. In the IPS analysis, however, the scintillation level is derived by calculating the power spectrum of the intensity time series and evaluating the fluctuation power within the frequency range corresponding to IPS. Consequently, intermittent RFI, particularly RFI containing fluctuations around 0.1–1 Hz that overlap the characteristic IPS frequency range, can lead to an overestimation of the derived IPS response.

A median filter was applied to remove short-duration impulsive RFI, and the resulting data with a temporal resolution of 20 ms were used for the IPS analysis. Although this procedure removes a substantial fraction of the RFI, strong interference cannot always be completely eliminated. Figure 2(a) shows the intensity time series of 0148+274 observed from 01:28:15 UT, for which a strong apparent IPS response was detected during the morning. Large impulsive fluctuations remained even after application of the median filter, suggesting that the derived IPS response may have been affected by residual RFI. Similar examinations of other radio sources indicate that some of the strongest IPS responses may also have been enhanced by residual interference. In contrast, Figure 2(b) shows the intensity time series of 0038+328 observed from 00:17:50 UT. The enhancement in 0038+328 was not accompanied by prominent impulsive RFI, although other forms of residual interference cannot be excluded. Therefore, although the absolute amplitudes of the IPS responses from individual radio sources should be interpreted with caution, the overall spatial distribution of the enhanced scattering observed on 10 May cannot be explained solely by RFI. The observations suggest that a broad region of interplanetary space was filled with plasma structures capable of producing enhanced radio-wave scattering.

Figure 2. Median-filtered 327 MHz intensity time series on 10 May 2024.

Uncalibrated 327 MHz output, expressed in analog-to-digital converter (ADC) counts, for radio sources observed by IPS on 10 May 2024: (a) 0148+274 and (b) 0038+328. The time series are shown after median filtering, with a temporal resolution of 20 ms.

3.3 Comparison with the SUSANOO-CME Simulation

To investigate the origin of the observed IPS enhancements, we compared the observations with synthetic IPS distributions calculated from the SUSANOO-CME simulation (Shiota and Kataoka, 2016;

Iwai et al., 2019, 2021). The results are shown in Figure 3. In the simulation, multiple CMEs launched after 8 May approached one another in interplanetary space and formed adjacent or partially merged high-density regions. These dense structures intersected IPS lines of sight over a broad range of directions and broadly reproduced the widespread IPS enhancements observed on 10 May.

Figure 3. Comparison of IPS observations and the SUSANOO-CME simulation at 01:00 UT on 10 May 2024.

Comparison between IPS observations and the SUSANOO-CME simulation at 01:00 UT on 10 May 2024. Right: An ecliptic-plane slice of the density distribution derived from the SUSANOO-CME simulation. The density from a background simulation without CMEs was subtracted, and the resulting density enhancement was normalized by the square of the heliocentric distance. The plotted quantity is $(n_{\mathrm{CME}} - n_{\mathrm{bg}})r^2$, where $n_{\mathrm{CME}}$and $n_{\mathrm{bg}}$are the plasma number densities in the simulations with and without CMEs, respectively, and r is the heliocentric distance. White lines show the projections of the IPS lines of sight onto the ecliptic plane. Left: Synthetic IPS g-levels calculated from the SUSANOO-CME simulation. Background colors represent the synthetic IPS g-levels, while symbols represent the observed IPS g-levels. An animation covering the event period is provided in Additional file 1.

One of the important results of the simulation is the formation of adjacent or partially merged dense regions through the propagation of successive CMEs. Multiple CMEs were launched after 8 May, and their interplanetary structures became closely packed along several lines of sight (Liu et al., 2024). Such neighboring or interacting disturbances can form dense structures over a broad region of the heliosphere and increase the number of viewing directions in which strong IPS responses are expected (Liu et al., 2014; Lugaz et al., 2017). This scenario provides a natural explanation for the widespread strong scattering observed on 10 May. The qualitative correspondence between the observed and synthetic IPS distributions is consistent with extended compression regions associated with successive CMEs, including possible CME–CME interactions.

The comparison also provides a physical explanation for the detection of strong IPS signatures over a wide range of solar elongations. In the simulation, the dense plasma regions were not confined to the immediate leading edge of a single CME. Instead, they were distributed within a more complex and spatially extended structure produced by multiple eruptions and their associated compression regions. When the lines of sight toward the radio sources crossed these regions, enhanced scattering was expected over a broad angular range (Manoharan, 2006). This is consistent with the detection of strong IPS responses not only close to the Sun but also toward radio sources located farther from the Sun in projection.

4. Discussion

The comparison between the IPS observations and the SUSANOO-CME simulation suggests that the May 2024 event was characterized not by a single isolated eruption, but by a complex interplanetary

disturbance formed by multiple successive CMEs (Liu et al., 2024; Razquin et al., 2025). The widespread IPS enhancements observed on 10 May, together with the spatially extended high-density regions reproduced in the simulation, indicate that multiple CME-related compression structures occupied a broad region of the inner heliosphere before the onset of the major geomagnetic storm at Earth (Figs. 1 and 3).

Both the observed IPS distribution and the simulation support a scenario in which successive CMEs formed adjacent or partially merged high-density regions during propagation (Liu et al., 2014; Liu et al., 2024). The formation of such structures increases the number of lines of sight intersecting compressed plasma regions and is therefore expected to produce strong IPS responses over a wide angular range. The present event thus provides an example showing that IPS observations are sensitive not only to individual CME fronts, but also to extended heliospheric disturbances formed by multiple eruptions and their possible interaction during propagation.

From a space weather perspective, this result is important. Severe geomagnetic disturbances can arise when multiple solar wind structures become compounded or interact during propagation (Webb and Howard, 2012; Liu et al., 2014; Lugaz et al., 2017). In the present event, strong IPS responses were detected on 9–10 May, before geomagnetic activity reached its maximum on 10–11 May. Although this study does not directly address operational forecasting, it demonstrates that IPS observations can detect large-scale interplanetary disturbances with potentially significant geoeffectiveness before their arrival at Earth (Iwai et al., 2019, 2021; Park et al., 2020). IPS may therefore provide useful information for the early recognition of complex CME events that could subsequently produce severe space weather.

The present study also has several limitations. First, the influence of residual RFIs cannot be completely excluded from the IPS data, and some of the strongest responses may have been affected by non-heliospheric contamination (Fig. 2). Residual RFI remains an important source of uncertainty in both the individual IPS amplitudes and the inferred spatial distribution of the enhancement.

Second, the agreement between the observations and the simulation is primarily qualitative, and clear discrepancies are found at some times and along some lines of sight. Figure 4 shows a comparison between the observations and the simulation at 07:00 UT on 10 May 2024. At this time, the simulated CME-related enhancement had not yet reached the region sampled by the strong observed IPS responses at solar elongations of approximately 1.0–1.2 rad (Fig. 4). The simulated enhancement reached this region approximately 10 h later (see Additional file 1).

Several factors may have contributed to this discrepancy. First, uncertainties in the background solar wind, particularly in the arrival time and spatial structure of the slow solar wind, may have affected the propagation speed and morphology of the CMEs. Differences in the background solar wind can influence not only the propagation of a CME, but also the deformation of its shape (Shiota and Kataoka, 2016). Second, the CMEs were represented as spheromak structures in the simulation. Although this simplified representation is useful for describing the large-scale propagation of CMEs, it may not fully reproduce the three-dimensional morphology of closely interacting eruptions, particularly their flank structures. The

spheromak model may therefore have limitations in describing the detailed shapes of CME flanks and the merging process of multiple CMEs. Third, the synthetic IPS calculation used in this study assumes a simple proportional relationship between the magnitude of electron density fluctuations and the electron density itself. This relationship may not necessarily hold in the complex plasma environment produced by interacting CMEs. In addition, waves or enhanced density fluctuations upstream of the shock may have increased the IPS response before the CME body or shock itself crossed the corresponding line of sight (Gothoskar and Rao, 1999). The discrepancy shown in Fig. 4 may therefore have resulted from a combination of uncertainties in the background solar wind, simplification of the CME morphology, and assumptions in the IPS scattering model.

These uncertainties do not invalidate the main conclusion of this study, but they highlight the need for a more quantitative integration of IPS observations with heliospheric MHD simulations. In particular, future improvements should include a more accurate specification of the background solar wind, more realistic representations of CME morphology, and synthetic IPS calculations that better account for the relationship between electron density and density fluctuations.

Despite these limitations, the present event demonstrates the observational value of IPS as a wide-angle remote-sensing technique for the inner heliosphere. White-light coronagraph observations are primarily sensitive to CMEs near the Sun, whereas detailed in situ measurements are available only at the limited locations of spacecraft (Webb and Howard, 2012). IPS fills the observational gap between these regimes by providing daily information on the distribution of heliospheric density disturbances over a broad range of solar elongations.

The May 2024 event shows that IPS observations are particularly useful when multiple CMEs propagate in close succession and form complex structures that are difficult to characterize using observations near the Sun or near Earth alone. If the integration of IPS data with heliospheric MHD simulations can be further improved for real-time applications, the locations, spatial extents, and interactions of successive CMEs may be constrained more reliably (Iwai et al., 2019, 2021). The present study can therefore be regarded as a case study that illustrates both the current capability and the remaining challenges of using IPS observations to monitor complex heliospheric disturbances with potentially significant impacts at Earth.

Figure 4. Comparison of IPS observations and the SUSANOO-CME simulation at 07:00 UT on 10 May 2024.

Comparison between the IPS observations and the SUSANOO-CME simulation at 07:00 UT on 10 May 2024. The format is the same as that of Fig. 3. Strong IPS responses were detected along several lines of sight, whereas no corresponding CME structure was reproduced at the same time and location in the simulation.

5. Conclusions

We investigated the large-scale inner-heliospheric disturbance associated with the May 2024 CME sequence using 327 MHz IPS observations and the SUSANOO-CME MHD simulation. On 9–10 May, particularly on 10 May, enhanced scintillation was detected along numerous lines of sight over a broad range of solar elongations before the main geomagnetic disturbance at Earth. The simulation broadly reproduced this widespread pattern as signatures of adjacent or partially merged compression regions formed during the propagation of successive CMEs. The combined results are therefore consistent with a compound, spatially extended CME-related disturbance rather than a single isolated CME front. The correspondence was qualitative, and residual RFI and an approximately 10 h discrepancy in the modeled timing limit the interpretation of individual lines of sight. Nevertheless, this event illustrates the value of combining IPS observations with heliospheric MHD modeling to identify the large-scale configuration of complex CME-related density disturbances before their arrival at Earth. More quantitative applications will require improved representations of the background solar wind and CME morphology, together with a more realistic synthetic IPS model.

Declarations

Ethics approval and consent to participate

Not applicable.

Consent for publication

Not applicable.

Availability of data and materials

The observational datasets used in this study are publicly available. The IPS data are available from the data repository of ISEE, Nagoya University (http://stsw1.isee.nagoya-u.ac.jp/ips_data-e.html), the LASCO data from the Virtual Solar Observatory (https://sdac.virtualsolar.org/cgi/search), and the in situ solar wind data from the OMNIWeb service (https://omniweb.gsfc.nasa.gov/). An animation of the simulation results is provided as Additional file 1.

Competing interests

The authors declare that they have no competing interests.

Funding

This work was supported by MEXT/JSPS KAKENHI Grant Numbers 24H00022, 22K18869, and 25K01052. The funding body had no role in the design of the study; the collection, analysis, or interpretation of the data; or the writing of the manuscript.

Authors' contributions

KI led this study and drafted the manuscript. DS developed the MHD simulation codes and derived CME parameters used in this study. KI, KF, and HI operated and maintained the IPS radio observations. DS operated and maintained the space weather forecasting system based on the MHD simulations. KI, DS, KF, and HI discussed the result of the IPS observations and the MHD simulations. All authors read and approved the final manuscript.

Acknowledgements

This work was supported by MEXT/JSPS KAKENHI Grant Numbers 24H00022, 22K18869, and 25K01052. The IPS observations were provided by the solar wind program of the Institute for Space-Earth Environmental Research (ISEE). This study was conducted using the computational resources of the Center for Integrated Data Science, ISEE, Nagoya University, through a joint research program. We thank the LASCO coronagraph group for the white-light CME images.

References

1. Gapper GR, Hewish A, Purvis A, Duffett-Smith PJ (1982) Observing interplanetary disturbances from the ground. Nature 296:633–636. https://doi.org/10.1038/296633a0
2. Glyantsev AV, Tyul'bashev SA, Chashei IV, Shishov VI (2015) Interplanetary-scintillation observations of coronal mass ejections near the maximum of the 24th solar-activity cycle. Astron Rep 59:40–45. https://doi.org/10.1134/S1063772915010047
3. Gothoskar P, Rao AP (1999) On observing mass ejections in the interplanetary medium. Sol Phys 185:361–390. https://doi.org/10.1023/A:1005114622634
4. Hayakawa H, Ebihara Y, Mishev A, Koldobskiy S, Kusano K, Bechet S et al (2025) The solar and geomagnetic storms in 2024 May: a flash data report. Astrophys J 979:49. https://doi.org/10.3847/1538-4357/ad9335
5. Hayashi K, Kojima M, Tokumaru M, Fujiki K (2003) MHD tomography using interplanetary scintillation measurement. J Geophys Res Space Phys 108:1102. https://doi.org/10.1029/2002JA009567
6. Hewish A, Scott PF, Wills D (1964) Interplanetary scintillation of small diameter radio sources. Nature 203:1214–1217. https://doi.org/10.1038/2031214a0
7. Iwai K, Shiota D, Tokumaru M, Fujiki K, Den M, Kubo Y (2019) Development of a coronal mass ejection arrival time forecasting system using interplanetary scintillation observations. Earth Planets Space 71:39. https://doi.org/10.1186/s40623-019-1019-5
8. Iwai K, Shiota D, Tokumaru M, Fujiki K, Den M, Kubo Y (2021) Validation of coronal mass ejection arrival-time forecasts by magnetohydrodynamic simulations based on interplanetary scintillation observations. Earth Planets Space 73:9. https://doi.org/10.1186/s40623-020-01345-5
9. Iwai K, Fallows RA, Bisi MM, Shiota D, Jackson BV, Tokumaru M et al (2023) Magnetohydrodynamic simulation of coronal mass ejections using interplanetary scintillation data observed from radio sites ISEE and LOFAR. Adv Space Res 72:5328–5340. https://doi.org/10.1016/j.asr.2022.09.028

10. Jackson BV, Hick PL, Kojima M, Yokobe A (1998) Heliospheric tomography using interplanetary scintillation observations: 1. Combined Nagoya and Cambridge data. J Geophys Res Space Phys 103:12049–12067. https://doi.org/10.1029/97JA02528
11. Jackson BV, Odstrcil D, Yu HS, Hick PP, Buffington A, Mejia-Ambriz JC et al (2015) The UCSD kinematic IPS solar wind boundary and its use in the ENLIL 3-D MHD prediction model. Space Weather 13:104–115. https://doi.org/10.1002/2014SW001130
12. Kojima M, Tokumaru M, Watanabe H, Yokobe A, Asai K, Jackson BV et al (1998) Heliospheric tomography using interplanetary scintillation observations: 2. Latitude and heliocentric distance dependence of solar wind structure at 0.1–1 AU. J Geophys Res Space Phys 103:1981–1989. https://doi.org/10.1029/97JA02162
13. Liu YD, Luhmann JG, Kajdič P, Kilpua EKJ, Lugaz N, Nitta NV et al (2014) Observations of an extreme storm in interplanetary space caused by successive coronal mass ejections. Nat Commun 5:3481. https://doi.org/10.1038/ncomms4481
14. Liu YD, Hu H, Zhao X, Chen C, Wang R (2024) A pileup of coronal mass ejections produced the largest geomagnetic storm in two decades. Astrophys J Lett 974:L8. https://doi.org/10.3847/2041-8213/ad7ba4
15. Lugaz N, Temmer M, Wang Y, Farrugia CJ (2017) The interaction of successive coronal mass ejections: a review. Sol Phys 292:64. https://doi.org/10.1007/s11207-017-1091-6
16. Manoharan PK (2006) Evolution of coronal mass ejections in the inner heliosphere: a study using white-light and scintillation images. Sol Phys 235:345–368. https://doi.org/10.1007/s11207-006-0100-y
17. Mlynczak MG, Hunt LA, Nowak N, Marshall BT, Mertens CJ (2024) Global thermospheric infrared response to the Mother's Day weekend extreme storm of 2024. Geophys Res Lett 51:e2024GL110701. https://doi.org/10.1029/2024GL110701
18. Park SR, Jeon HC, Kim RS, Kim JH, Kim SJ, Cho J et al (2020) Development of forecast algorithm for coronal mass ejection speed and arrival time based on propagation tracking by interplanetary scintillation g-value. J Astron Space Sci 37:43–50. https://doi.org/10.5140/JASS.2020.37.1.43
19. Razquin A, Veronig AM, Dissauer K, Podladchikova T, Jain S (2025) Coronal dimmings from active region 13664 during the May 2024 solar energetic events. Astron Astrophys 699:A40. https://doi.org/10.1051/0004-6361/202554772
20. Sakaguchi K, Akiyama S, Andoh S, Bamba Y, Enoki K, Park I et al (2026) Evaluation of NICT space weather forecast for extreme events in May 2024. Earth Planets Space 78:178. https://doi.org/10.1186/s40623-026-02501-z
21. Shiota D, Kataoka R, Miyoshi Y, Hara T, Tao C, Masunaga K et al (2014) Inner heliosphere MHD modeling system applicable to space weather forecasting for the other planets. Space Weather 12:187–204. https://doi.org/10.1002/2013SW000989
22. Shiota D, Kataoka R (2016) Magnetohydrodynamic simulation of interplanetary propagation of multiple coronal mass ejections with internal magnetic flux rope (SUSANOO-CME). Space Weather

14:56–75. https://doi.org/10.1002/2015SW001308

23. Spogli L, Alberti T, Bagiacchi P, Cafarella L, Cesaroni C, Cianchini G et al (2024) The effects of the May 2024 Mother's Day superstorm over the Mediterranean sector: from data to public communication. Ann Geophys 67:PA218. https://doi.org/10.4401/ag-9117
24. Tokumaru M, Kojima M, Fujiki K, Maruyama K, Maruyama Y, Ito H et al (2011) A newly developed UHF radiotelescope for interplanetary scintillation observations: Solar Wind Imaging Facility. Radio Sci 46:RS0F02. https://doi.org/10.1029/2011RS004694
25. Tulasi Ram S, Veenadhari B, Dimri AP, Bulusu J, Bagiya M, Gurubaran S et al (2024) Super-intense geomagnetic storm on 10–11 May 2024: possible mechanisms and impacts. Space Weather 22:e2024SW004126. https://doi.org/10.1029/2024SW004126
26. Webb DF, Howard TA (2012) Coronal mass ejections: observations. Living Rev Sol Phys 9:3. https://doi.org/10.12942/lrsp-2012-3
27. Young AT (1971) Interpretation of interplanetary scintillations. Astrophys J 168:543. https://doi.org/10.1086/151108
28. Yu HS, Jackson BV, Hick PP, Buffington A, Odstrčil D, Wu CC et al (2015) 3D reconstruction of interplanetary scintillation (IPS) remote-sensing data: global solar wind boundaries for driving 3D-MHD models. Sol Phys 290:2519–2538. https://doi.org/10.1007/s11207-015-0685-0

Figures

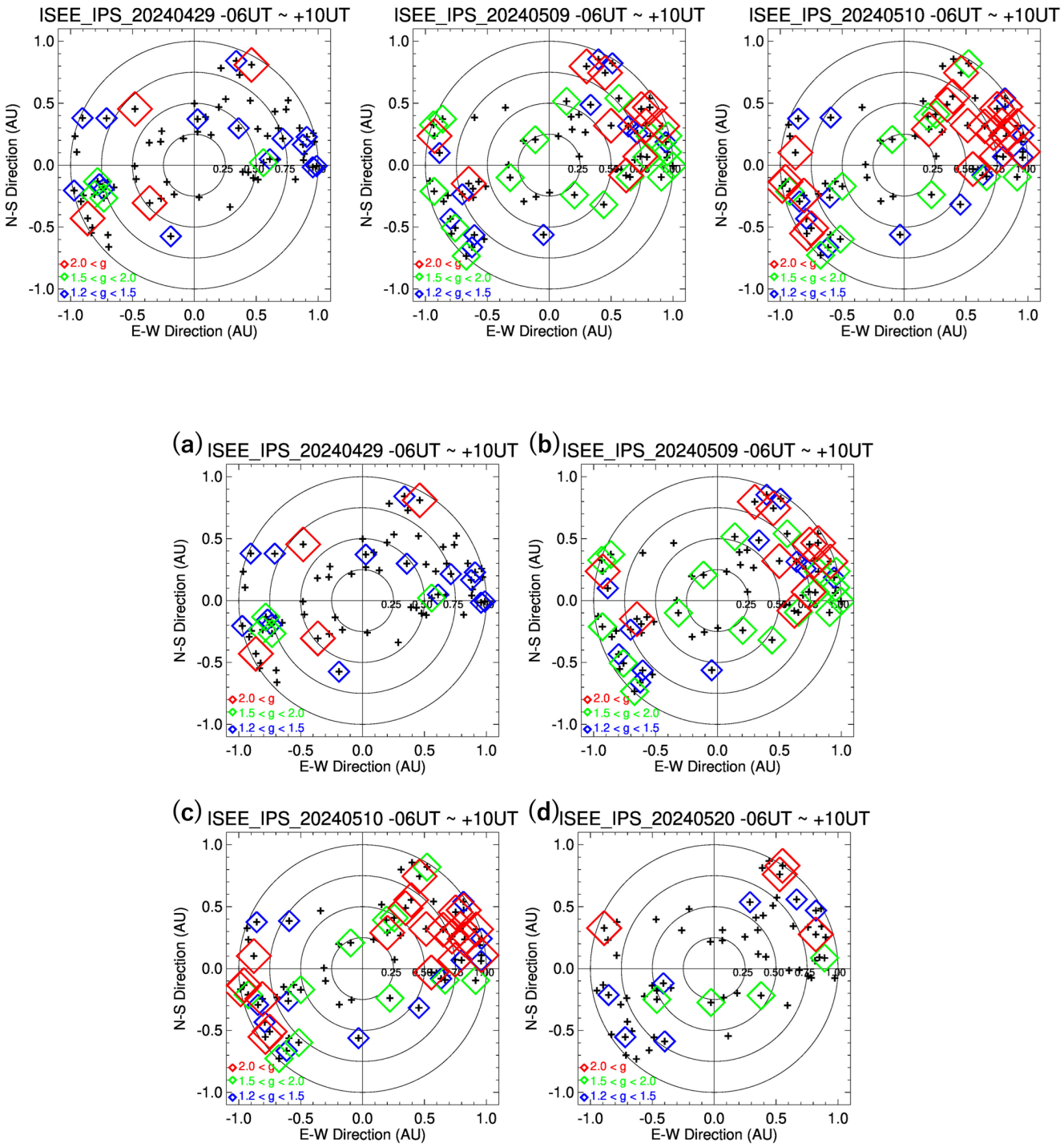

Figure 1

IPS sky maps before, during, and after the May 2024 CME event.

All-source IPS sky maps observed on (a) 29 April, (b) 9 May, (c) 10 May, and (d) 20 May 2024. The center of each panel corresponds to the Sun, and the horizontal and vertical axes indicate the east–west and north–south positions of the P-points (the points of closest approach of the lines of sight to the Sun),

expressed in AU. Plus signs indicate lines of sight toward the observed radio sources. Diamonds represent IPS g-levels: red for (g > 2.0), green for (1.5 < g < 2.0), and blue for (1.2 < g < 1.5).

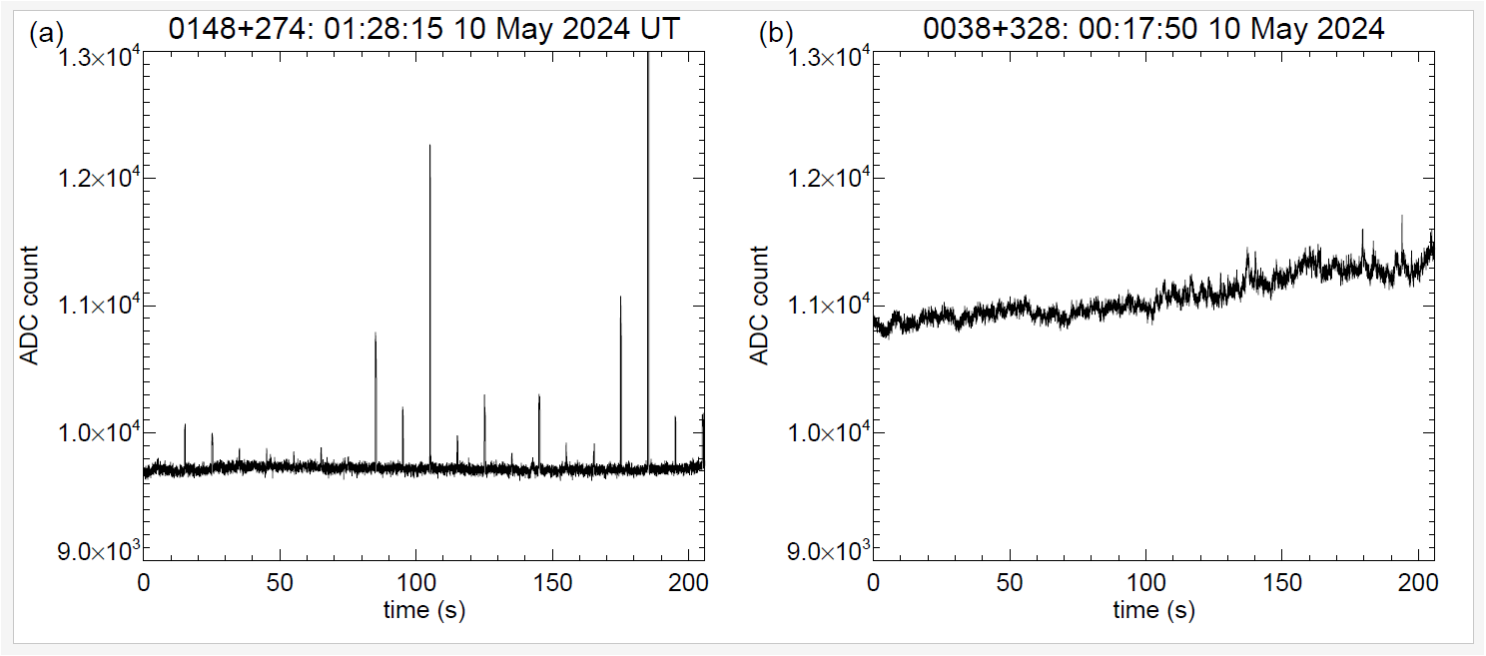

Figure 2

Median-filtered 327 MHz intensity time series on 10 May 2024.

Uncalibrated 327 MHz output, expressed in analog-to-digital converter (ADC) counts, for radio sources observed by IPS on 10 May 2024: (a) 0148+274 and (b) 0038+328. The time series are shown after median filtering, with a temporal resolution of 20 ms.

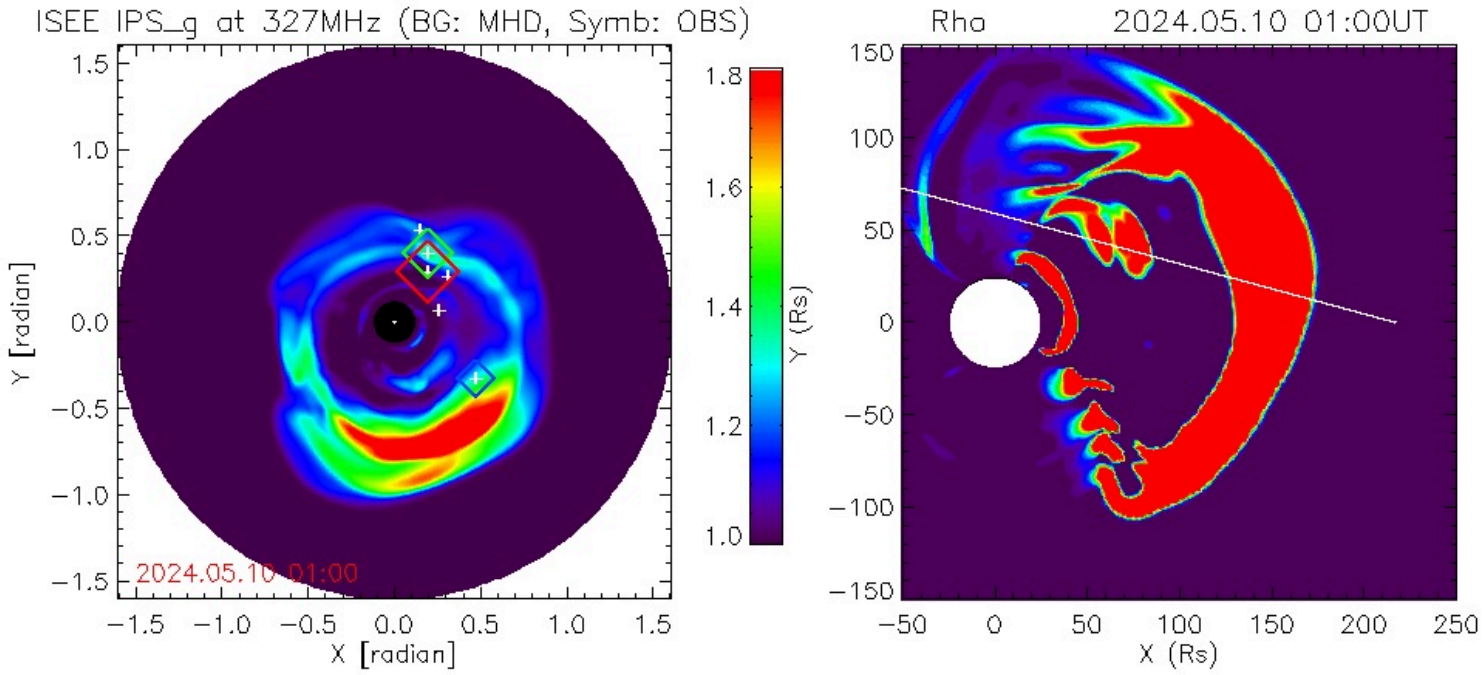

Figure 3

Comparison of IPS observations and the SUSANOO-CME simulation at 01:00 UT on 10 May 2024.

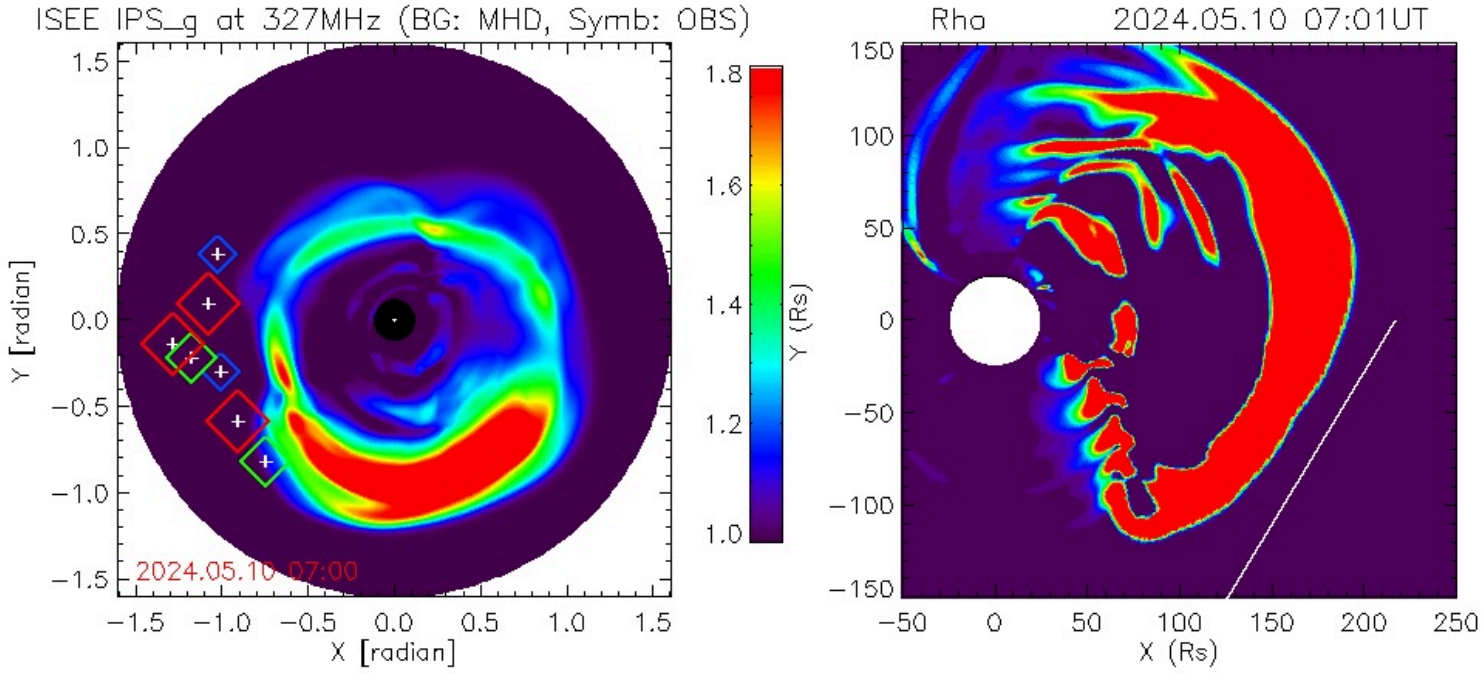

Figure 4

Comparison of IPS observations and the SUSANOO-CME simulation at 07:00 UT on 10 May 2024.

Comparison between the IPS observations and the SUSANOO-CME simulation at 07:00 UT on 10 May 2024. The format is the same as that of Figure 3. Strong IPS responses were detected along several lines of sight, whereas no corresponding CME structure was reproduced at the same time and location in the simulation.

Supplementary Files

This is a list of supplementary files associated with this preprint. Click to download.

- AdditionalFile1.1.mp4
- GA.png